

Fast Nonlinear Ion Transport via Field-Induced Hydrodynamic Slip in Sub-20-nm Hydrophilic Nanofluidic Transistors

Udi Vermesh,^{†,‡} Jang Wook Choi,^{†,§,||} Ophir Vermesh,[§] Rong Fan,[§] John Nagarah,[§] and James R. Heath^{*,§}

The Kavli Nanoscience Institute and Division of Engineering and Applied Science, Bioengineering, Caltech, Pasadena, California 91125, and Division of Chemistry and Chemical Engineering, Caltech, Pasadena, California 91125

Received September 25, 2008; Revised Manuscript Received January 9, 2009

ABSTRACT

Electrolyte transport through an array of 20 nm wide, 20 μm long SiO_2 nanofluidic transistors is described. At sufficiently low ionic strength, the Debye screening length exceeds the channel width, and ion transport is limited by the negatively charged channel surfaces. At source–drain biases >5 V, the current exhibits a sharp, nonlinear increase, with a 20–50-fold conductance enhancement. This behavior is attributed to a breakdown of the zero-slip condition. Implications for energy conversion devices are discussed.

Recently, novel fluid-mechanical phenomena have been observed as the dimensions of fluidic channels have approached the nanometer scale. Theoretical models^{1–4} and experimental demonstrations^{5–7} of finite hydrodynamic slip in hydrophobic nanochannels have received considerable attention. In particular, the relatively recent emergence of nanochannel fabrication methods^{8–10} has allowed electrokinetic phenomena to be investigated in nanofluidic systems and has created renewed interest in the potential of fluidic devices for energy conversion and other tasks. As the Debye screening length approaches the scale of the channel dimensions, the surface charge dominates the electrokinetic flow behavior within the channel, controlling the concentration of electrolytes^{11–16} such that unipolar counterions dominate current flow. This phenomenon can potentially be harnessed for mechanical-to-electrical energy conversion by using pressure to drive a streaming current through the nanochannel. Alternatively, electrical-to-mechanical energy conversion is possible by applying an electric field across the length of the nanochannel, thereby driving fluid through by electroosmosis. However, current flow through nanofluidic channels at a given pressure, or source–drain voltage, is severely limited due to the no-slip boundary condition that characterizes most such systems. This boundary condition represents the fact that there is no fluid or ion flow at the liquid/channel interface. The counterion density is highest at this interface,

but because these counterions are immobilized by surface charges, those ions do not contribute to the current, resulting in low energy conversion efficiencies.

The no-slip boundary condition is not a fundamental limitation, however, and systems with finite slip have received recent attention.^{17,18} Slip velocity (v_{slip}) is proportional to the shear rate, according to the following equation

$$v_{\text{slip}} = \mathbf{b}(dv/dx) \Big|_{\text{surf}}$$

Here, \mathbf{v} is the fluid velocity, \mathbf{x} is the coordinate normal to the surface, and \mathbf{b} is the slip length, or the distance into the surface where \mathbf{v} extrapolates to zero. A number of theoretical studies^{18,19} have revealed that mechanical-to-electrical energy conversion efficiencies can be very high, even approaching 100%, for nanofluidic channels exhibiting a large \mathbf{b} . These studies have focused on streaming currents through smooth, hydrophobic nanofluidic channels, since such systems are thought to exhibit the greatest potential for slip. For example, Ren and Stein¹⁸ have calculated that, for a 10 nm high slit-shaped, hydrophobic nanochannel, 40% energy conversion efficiencies are realistic for \mathbf{b} values of 30 nm. Indeed, very large slip lengths have been measured in carbon-nanotube-based nanofluidic channels.^{5,7} However such devices may not be suitable for energy conversion since the lack of surface charges prevents the creation of an intrachannel unipolar environment essential for mechanical-to-electrical energy conversion. Currently, most nanofluidic channels are fabricated from silica or other materials that yield charged and

* Corresponding author, heath@caltech.edu.

[†] These authors contributed equally to this work.

[‡] Division of Engineering and Applied Science, Bioengineering.

[§] Division of Chemistry and Chemical Engineering.

^{||} Present address: Department of Materials Science and Engineering, Stanford University, Stanford, CA 94305.

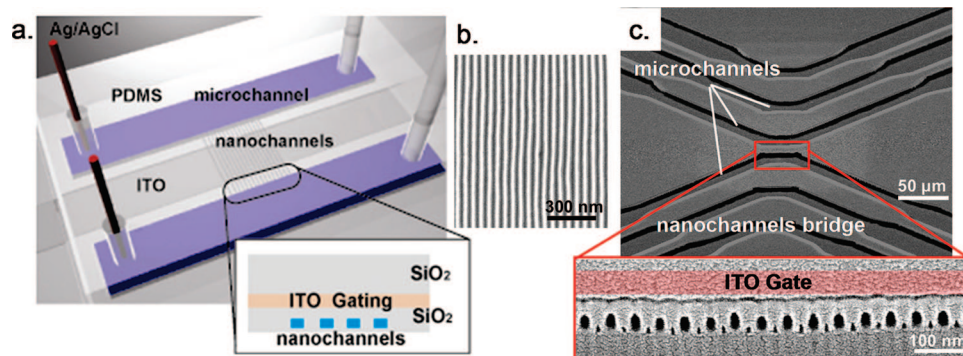


Figure 1. Overview of nanofluidic device. (a) Experimental setup of essential components of the nanofluidic transistor array. The blue microchannels are electrically contacted with Ag/AgCl source and drain electrodes. These microchannels are connected via a bridge of 80 nanofluidic channels in SiO₂. As shown in the inset, the nanochannels are topped with an ITO gate electrode. (b) Scanning electron micrograph (SEM) of the silicon nanowire array (top view) from which the SiO₂ nanochannels were templated. (c) SEM of the nanofluidic device. The six V-shaped structures are microfluidic channels; only the two opposing microchannels in the central region of the image are utilized for these experiments. These two channels are bridged by the 20 μm long nanofluidic channel array. Below, an end-on SEM view of a few of the (20 nm wide × 30 nm high) nanofluidic channels is shown, with the position of the ITO gate electrode indicated.

or hydrophilic surfaces. Due to the strong attraction of Stern layer counterions to such hydrophilic surfaces, the no-slip condition is difficult to overcome. For example, Dekker's group has measured energy conversion in hydrophilic nanochannels under no-slip conditions and found a conversion efficiency of only 3%.²⁰ They calculated a maximum conversion efficiency of 12% for similar monovalent ions in water.¹⁹ Much greater conversion efficiencies will be needed for practical technologies to be realized. If the no-slip boundary condition in hydrophilic channels could be surmounted, greatly enhanced streaming currents and energy conversion efficiencies would be possible in such systems, making energy conversion applications far more feasible.

In this paper, we report on the electrokinetics of KCl ion transport through nanofluidic transistors comprised of arrays of oval-shaped, 20 nm wide, hydrophilic, silica nanochannels. Although ion transport has been investigated previously in a single SiO₂ nanofluidic channel¹⁰ with similarly small dimensions, our fabrication method²¹ produces sufficiently large numbers of closely spaced SiO₂ nanochannels such that currents can be measured even at very low KCl molarities ([KCl] = 10⁻⁷ M). The experimental setup is shown in Figure 1. The nanofluidic device consisted of a 20 μm long array of 80 parallel, 20 nm × 30 nm cross section silica channels built from a template of silicon nanowires fabricated using the SNAP method²¹ (Figure 1b,c). An indium tin oxide (ITO) gate electrode is deposited on top of the array, with a silica gate oxide layer sandwiched in between. As shown in Figure 1c, extremely narrow (~3 nm) channels between the primary channels were observed. These likely arise from a SiO₂ deposition process that is not 100% conformal. However, the voids are far smaller than the primary nanochannels and their contribution to the ionic current should be negligible. The nanochannels interface with two sets of microfluidic channels that act as reservoirs for electrolyte solutions. The device is sealed with a slab of plasma-bonded PDMS to isolate the microfluidic channels and prevent leakage current. Finally, holes are punched into the PDMS to allow the insertion of Ag/AgCl electrodes into the microfluidic channels for current measurements. The detailed fabrication

processes are described in the Supporting Information. The SNAP-based nanochannel fabrication method is robust, allowing devices to be consistently generated with nearly 100% yield.

Upon completion of device fabrication, we introduced aqueous solutions of KCl into the device at concentrations ranging from 10⁻⁷ to 10⁻¹ M, optically observed nanochannel filling over the entire array, and measured the source–drain current–voltage ($I-V_{SD}$) characteristics over a 30–50 V range. (Conductance plots (dI/dV_{SD}) at the above-mentioned KCl concentrations, as well as for additional KCl concentrations between 10⁻² and 10⁻³ M, are presented in the Supporting Information.) Similar to previous studies,^{12,13} which were limited to conductance measurements at low bias (<5 V), conductance saturation is present below a threshold concentration of 2.5×10^{-3} M. Conductance saturation occurs because the negatively charged silanol groups at the SiO₂ nanochannel surface attract K⁺ counterions and repel Cl⁻ anions over the characteristic Debye length (κ^{-1}), which is given by²²

$$\kappa^{-1} = [\epsilon k_B T / (e^2 N_A \sum_i c_i Z_i^2)]^{1/2}$$

Here, c_i is the molar concentration and Z_i is the valence of ion species i . Standard constants include ϵ (the permittivity), k_B (Boltzmann constant), e (electron charge), and N_A (Avogadro's number). For [KCl] = 10⁻³ M, this gives a Debye length of 9.7 nm, which is comparable to the 10 nm radius of our nanochannels. As a result, the K⁺ concentration within our nanochannels is determined by the surface charge on the walls for bulk [KCl] ≤ 10⁻³ M. On the other hand, for [KCl] > 10⁻³ M, the Debye length becomes smaller than the nanochannel radius, leading to shielding of surface charges, more Ohmic ion transport behavior (Figure 2b), and a conductance that scales approximately linearly with [KCl] (Supplementary Figure 6 and Supplementary Table 1 in Supporting Information).

In the surface-charge-governed ion transport regime, [KCl] ≤ 10⁻³ M, and for V_{SD} values above a threshold voltage (V_T) of about 5 V, the current exhibits a sharp and nonlinear

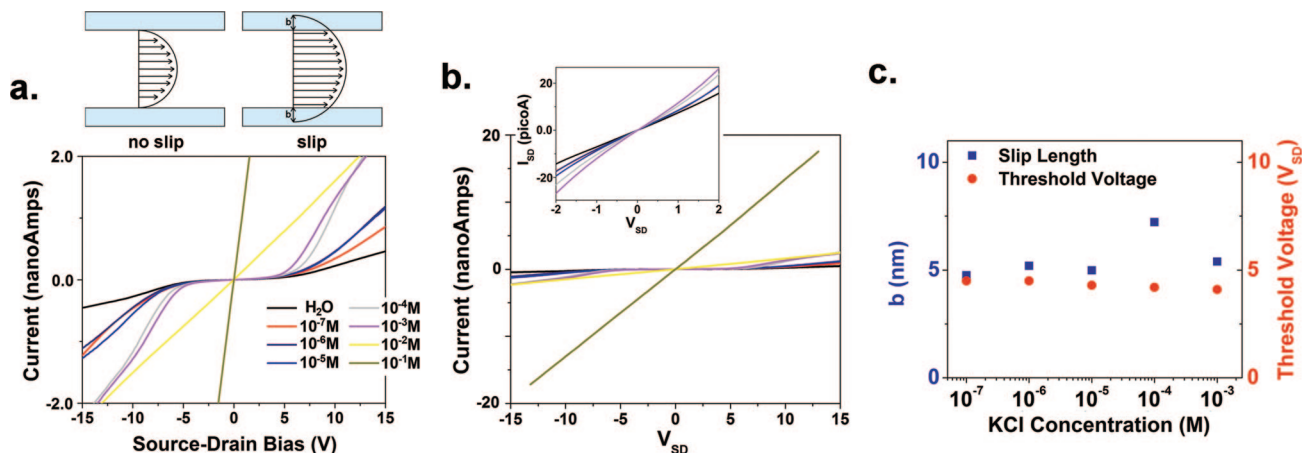


Figure 2. Source–drain current–voltage (I – V) data of the nanofluidic devices at various values of [KCl]. (a) I – V curves for [KCl] from 10^{-7} to 10^{-1} M. The sharp increase in conductance at $V_{SD} \sim 5$ V for all curves for which [KCl] $\leq 10^{-3}$ M is interpreted as the onset of nonzero slip. Schematic diagrams show ion velocity profiles in both the low bias no-slip region and the high bias slip region. (b) Source–drain I – V data plotted with an expanded current axis, illustrating conductance saturation for [KCl] $\leq 10^{-3}$ M. The saturation implies that, for those concentrations, the Debye screening length in the channel is larger than the channel width. Inset: Expanded I – V curves for [KCl] $\leq 10^{-3}$ M. Note the y-axis scale is picoamperes. The color coding of the traces is the same as in part a. (c) Slip length (**b**) vs KCl concentration for [KCl] $\leq 10^{-3}$ M along with a display of the threshold voltage (V_T) above which slip occurs with respect to these same KCl concentrations.

increase with increasing bias (Figure 2a) and conductance enhancement of 20–50-fold, depending upon [KCl]. We propose that this nonlinear behavior arises from an electric-field-induced breakdown of the zero-slip condition. The transition into the finite-slip regime can be attributed to the changing behavior of the K^+ ion double layer in the nanochannel solution. The layer closest to the surface, called the Stern layer, is about 0.3 nm thick²³ and consists of K^+ ions immobilized to the nanochannel surface. The second layer, which can move under no-slip conditions, is a diffuse layer of K^+ ions that comprises the rest of the solution within the nanochannels.²⁴ However, it has been theorized that the Stern layer can be moved tangential to the surface under the influence of an external electric field.^{2,23} In our device, this may be happening above the threshold V_{SD} , in which case the electric field parallel to the nanochannel surface is overcoming the attraction of the Stern layer K^+ ions to the silica surface. As a result, these ions move along the surface, electroosmotically pulling water with them, and the zero-slip condition no longer holds. Due to viscous forces, hydrodynamic slip at the nanochannel surface increases the velocity of all species within the nanochannel, resulting in greatly enhanced conductance as illustrated in the schematic diagrams in Figure 2a.

Nonlinear I – V characteristics in somewhat larger (40 nm deep) nanofluidic channels for sodium phosphate concentrations in the range 10^{-4} – 10^{-2} M have been observed by Kim et al.⁹ However, their results reflect very different physics. They observed a broad, current-saturated, intermediate bias region separating their low- and high-bias regions. They interpret their data within the framework of concentration polarization, in which an ion depletion region develops at the microchannel/nanochannel interface, which leads to the current saturation regime in their I_{SD} – V_{SD} plots. At sufficiently high bias, instabilities (imaged as vortices) appear at the microchannel/nanochannel interface, collapsing the depletion regions, and resulting in a second phase of steep

current increase (the overlimiting region). At even higher bias, conductance values return to their original (low-bias) levels. The lack of a current-saturated region in our data, the fact that conductances remain high and stable as V_{SD} increases, the absence of nonlinear ion transport above 10^{-3} M, and the below-described voltage-gating experiments all distinguish our system and support the interpretation of nonzero slip in our channels.

The contribution of slip to conductance enhancement within a nanochannel of radius comparable to the Debye screening length can be modeled as follows (see Supporting Information for detailed description). To maintain electroneutrality, the nanochannel surface charge must equal the counterion charge in the solution ($Q_{\text{surface}} = Q_{\text{solution}}$). This is expressed as

$$\mathbf{A} \times \boldsymbol{\sigma} = \mathbf{V} \times \mathbf{e} \times \mathbf{n}_{\text{cr}} \quad (1)$$

where \mathbf{A} is the nanochannel surface area, $\boldsymbol{\sigma}$ is the surface charge density, \mathbf{V} is the nanochannel volume, and \mathbf{n}_{cr} is the critical ion density at which nanochannel ion transport transitions from bulklike to a surface-charge governed regime (herein, \mathbf{n}_{cr} is equivalent to a K^+ concentration of $\sim 10^{-3}$ M). The value of $\boldsymbol{\sigma}$ obtained is 0.0006 C/m^2 . Using this value, the slip length \mathbf{b} can be calculated using the conductance equation

$$\mathbf{G} = \mathbf{N} \times 4\mu\sigma(\mathbf{d}/\mathbf{L})(1 + \mathbf{b}/l_{\text{Stern}}) \quad (2)$$

where μ is the K^+ mobility ($=7.6 \times 10^{-8} \text{ m}^2/(\text{V}\cdot\text{s})$), \mathbf{d} is the nanochannel hydraulic diameter ($=24 \text{ nm}$), \mathbf{L} is the nanochannel length ($=20 \mu\text{m}$), \mathbf{N} is the number of nanochannels (80) in the array, and l_{Stern} is the thickness of the Stern layer ($\sim 0.3 \text{ nm}$), which is also the distance over which the shear plane moves when shifting from no-slip to slip conditions. The first part of eq 2, $\mathbf{N} \times 4\mu\sigma(\mathbf{d}/\mathbf{L})$, represents electrokinetic conductance through the nanochannels in the absence of slip,

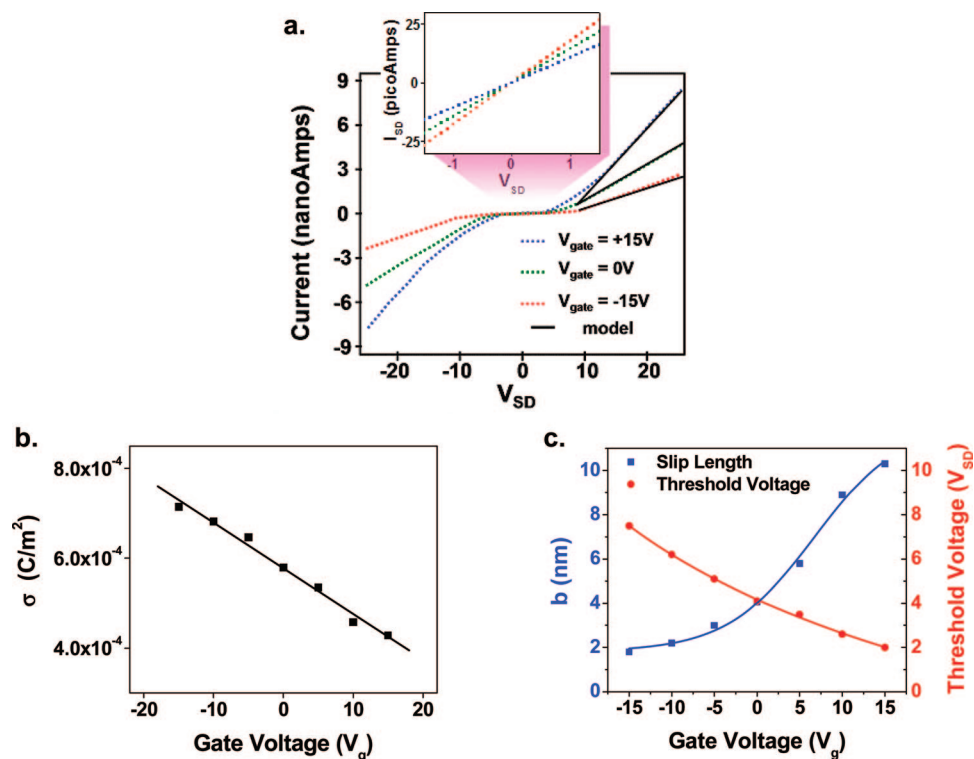


Figure 3. The influence of gate voltage (V_g) on the nanofluidic device at $[KCl] = 10^{-4}M$. (a) Source–drain current (I_{SD}) versus source–drain voltage (V_{SD}) at various values of V_g . At high source–drain bias, conductance increases as V_g becomes more positive. The fits utilize the full conductance equation, including the slip term. Inset: $I_{SD}-V_{SD}$ plot as zoomed in to the low source–drain bias region. Opposite to the trend seen in the high source–drain bias region, conductance decreases with more positive V_g . (b) Dependence of surface charge density (σ) on V_g . (c) Dependence of the slip length (b) and threshold voltage (V_T) (above which slip occurs) with respect to V_g .

and the $(1 + b/l_{Stern})$ factor represents the conductance enhancement due to slip.^{1,2} For conductance in the low bias ($V_{SD} < V_T$) regime, where there is no slip ($b = 0$), the measured conductance (~ 14.4 pS) is almost identical to the value calculated (~ 16.8 pS) using eqs 1 and 2.

If the emergence of hydrodynamic slip is indeed a consequence of a field-induced breakdown in electrostatic attractions between the Stern layer and the channel wall, reducing the surface charge density should lower this electrostatic barrier and enhance slip. This reasoning is supported by two observations. First, there is no significant difference either in slip length or in the threshold voltage at which slip occurs for all values of $[KCl] \leq 10^{-3} M$ (Figure 2c). This is attributable to the fact that the surface charge density remains fairly stable throughout these concentrations. Additional support stems from experiments that exploit a gate electrode to tune the nanochannel surface charge density and measure the corresponding change in slip length. The gating experiments on a $10^{-4} M$ KCl solution are presented in Figure 3. Identical experiments were carried out on a $10^{-4} M$ aspartic acid solution (see Supporting Information). The leakage current through the gate electrode was measured to be 500 fA at V_{SG} values of 5, 10, and 15 V, which is negligible compared to the measured source–drain current in the plots of Figure 3a (see Supplementary Figure 7 in Supporting Information).

Another noteworthy observation is the reversal in the effect of V_g on conductance between the low bias and high bias regimes. As V_g becomes more positive, the bare surface charge

density (σ) extracted from eq 1 becomes less negative (Figure 3b), which has two potentially competing effects. The first is a decrease in the intrachannel counterion concentration, which tends to *decrease* the conductance. The second is a decrease in the attraction of the Stern layer to the channel surface, which tends to *increase* the conductance (due to slip). At low source–drain bias ($V_{SD} < V_T$), the electric field is not strong enough to overcome the attraction of the Stern layer to the surface, so the decrease in ion concentration with increased V_g (Figure 3a inset) translates directly to a decreased conductance, as shown in previous studies.^{11,12} By contrast, in the high source–drain bias ($V_{SD} > V_T$) regime, the electric field is strong enough to move the Stern layer. Therefore, as V_g becomes more positive, the Stern layer moves faster (larger slip length, b) (Figure 3c), resulting in a net increase in conductance. Alternatively, less force is required to begin moving the Stern layer (lower V_T) as its attraction to the channel surface decreases with more positive V_g .

Over the entire range of V_{SD} , the nonlinear nature of the $I-V$ curves is evident for all values of V_g (Figure 3a). In the low bias regime ($V_{SD} < V_T$), where there is no slip, the Ohmic response is well-described by the conductance equation without the enhancement factor (notice that the enhancement factor reduces to unity for $b = 0$) as shown in the Supporting Information. In the high V_{SD} regime ($V_{SD} > V_T$), these curves were fitted with the full conductance equation including the slip enhancement term illustrated in eq 2. Such linear fits permitted us to extract the slip length, b , for each value of

V_g (Figure 3c). Our obtained slip lengths in the range of ~ 2 – 10 nm are comparable to those proposed in studies of SiO_2 surfaces²⁵ and represent on average 8–35-fold increases in conductance.

The ability to access finite-slip conditions in these nanochannels is encouraging from the point of view of energy conversion. We consider the mechanical power output of our device. This is the kinetic energy per unit time that is associated with the electroosmotic movement of fluid through the nanochannel array

$$\text{mechanical power} = (1/2)(\rho v_{\text{eof}} \mathbf{A}) v_{\text{eof}}^2 \quad (3)$$

where v_{eof} is the electroosmotic fluid velocity of water through the nanochannels, and $\rho v_{\text{eof}} \mathbf{A}$ is the mass flow rate. According to eq 3, the mechanical power increases as the cube of the electroosmotic fluid velocity. Therefore, an 80–200-fold increase in fluid velocity, as calculated in our device due to slip, translates to a $\sim 10^6$ enhancement in mechanical power. Detailed calculations on electroosmotic fluid velocity enhancements extracted from current measured in the nanochannel array device and their correlation to mechanical power are described in the Supporting Information. Such a large improvement in mechanical power through these silica channels suggests that they may be useful for certain applications for which nanofluidic devices have been targeted, such as filtration and water desalination.

On the basis of our results showing enhanced ion transport, silica-based nanofluidic devices would likely exhibit a higher mechanical-to-electrical energy conversion efficiency than the current measured limit of 3%.²⁰ In a recent work by Ren and Stein,¹⁸ theoretical characterization of electrokinetic transport through nanochannels showed that streaming current increases dramatically with increases in slip length, predicting >70% energy conversion efficiencies. The ability to tune slip lengths with gate voltages should permit the testing of this theory in future experiments. Measurements of streaming currents through nanochannels will require a slight modification of our device design, since the PDMS/silica interface cannot tolerate high pressures.

In summary, we have investigated ion transport through an array of 80 closely spaced sub-20-nm hydrophilic SiO_2 nanochannels over a 30–50 V range of source–drain biases. We have observed that for ion concentrations at which the Debye length exceeds the nanochannel radius, ion transport becomes greatly magnified at a threshold source–drain bias. This behavior can be described by a theoretical model that attributes the enhancement to a breakdown of the no-slip boundary condition at the liquid/nanochannel surface interface at high source–drain bias. By varying the surface charge density of the nanochannels using a gate electrode, we were able to tune the slip length to obtain further enhancements in ion transport through the hydrophilic nanochannel array. These results imply that such devices can be harnessed for efficient energy conversion applications.

Acknowledgment. This work was funded by the Department of Energy (DE-FG02-04ER46175) and by a subcontract

from the MITRE Corporation. U.V. acknowledges a Betty and Gordon Moore fellowship. J.W.C. acknowledges the Samsung Scholarship.

Supporting Information Available: Description of nanochannel fabrication and measurement, conductance equation derivation, and mechanical power calculations. This material is available free of charge via the Internet at <http://pubs.acs.org>.

References

- (1) Bocquet, L.; Barrat, J. L. Flow boundary conditions from nano- to micro-scales. *Soft Matter* **2007**, *3*, 685–693.
- (2) Joly, L.; Ybert, C.; Trizac, E.; Bocquet, L. Liquid friction on charged surfaces: from hydrodynamic slippage to electrokinetics. *J. Chem. Phys.* **2006**, *125*, 204716.
- (3) Joseph, S.; Aluru, N. R. Why are carbon nanotubes fast transporters of water. *Nano Lett.* **2008**, *8*, 452–458.
- (4) Netz, R. R. Electrofriction and dynamic Stern layers at planar charged surfaces. *Phys. Rev. Lett.* **2003**, *91*, 138101.
- (5) Holt, J. K.; et al. Fast mass transport through sub-2-nanometer carbon nanotubes. *Science* **2006**, *312*, 1034–1037.
- (6) Lee, C.; Choi, C.; Kim, C. Structured surfaces for a giant liquid slip. *Phys. Rev. Lett.* **2008**, *101*, 064501.
- (7) Majumder, M.; Chopra, N.; Andrews, R.; Hinds, B. J. Nanoscale hydrodynamics: enhanced flow in carbon nanotubes. *Nature* **2005**, *438*, 44–44.
- (8) Cao, H.; et al. Fabrication of 10 nm enclosed nanofluidic channels. *Appl. Phys. Lett.* **2002**, *81*, 174–176.
- (9) Kim, S. J.; Wang, Y. C.; Lee, J. H.; Jang, H.; Han, J. Concentration polarization and nonlinear electrokinetic flow near a nanofluidic channel. *Phys. Rev. Lett.* **2007**, *99*, 044501.
- (10) Liang, X. G.; Morton, K. J.; Austin, R. H.; Chou, S. Y. Single sub-20 nm wide, centimeter-long nanofluidic channel fabricated by novel nanoimprint mold fabrication and direct imprinting. *Nano Lett.* **2007**, *7*, 3774–3780.
- (11) Fan, R.; Yue, M.; Karnik, R.; Majumdar, A.; Yang, P. D. Polarity switching and transient responses in single nanotube nanofluidic transistors. *Phys. Rev. Lett.* **2005**, *95*, 086607.
- (12) Karnik, R.; et al. Electrostatic control of ions and molecules in nanofluidic transistors. *Nano Lett.* **2005**, *5*, 943–948.
- (13) Stein, D.; Kruithof, M.; Dekker, C. Surface-charge-governed ion transport in nanofluidic channels. *Phys. Rev. Lett.* **2004**, *93*, 035901.
- (14) Powell, M. R.; et al. Nanoprecipitation-assisted ion current oscillations. *Nat. Nanotechnol.* **2008**, *3*, 51–57.
- (15) Vlasiouk, I.; Siwy, Z. Nanofluidic diode. *Nano Lett.* **2007**, *7*, 552–556.
- (16) Kalman, E.; Vlasiouk, I.; Siwy, Z. Nanofluidic bipolar transistor. *Adv. Mater.* **2008**, *20*, 293–297.
- (17) Pennathur, S.; Eijkel, J. C.; van den Berg, A. Energy conversion in microsystems: is there a role for micro/nanofluidics. *Lab Chip* **2007**, *7*, 1234–1237.
- (18) Ren, Y. Q.; Stein, D. Slip-enhanced electrokinetic energy conversion in nanofluidic channels. *Nanotechnology* **2008**, *19*, 195707.
- (19) Van der Heyden, F. H. J.; Bonthuis, D. J.; Stein, D.; Meyer, C.; Dekker, C. Electrokinetic energy conversion efficiency in nanofluidic channels. *Nano Lett.* **2006**, *6*, 2232–2237.
- (20) Van der Heyden, F. H. J.; Bonthuis, D. J.; Stein, D.; Meyer, C.; Dekker, C. Power generation by pressure-driven transport of ions in nanofluidic channels. *Nano Lett.* **2007**, *7*, 1022–1025.
- (21) Melosh, N. A.; et al. Ultrahigh-density nanowire lattices and circuits. *Science* **2003**, *300*, 112–115.
- (22) Chun, M. S.; Park, W. C. Time evolution of electrokinetic flow-induced streaming potential and flux in dead-end and cross-flow filtration of colloids through nanopores. *J. Membr. Sci.* **2004**, *243*, 417–424.
- (23) Gupta, A. K.; Coelho, D.; Adler, P. M. Influence of the Stern layer on electrokinetic phenomena in porous media. *J. Colloid Interface Sci.* **2007**, *316*, 140–159.
- (24) Fawcett, W. R. *Liquids, Solutions, and Interfaces: From Classical Macroscopic Descriptions to Modern Microscopic Details (Topics in Analytical Chemistry)*; Oxford University Press: Oxford, 2004.
- (25) Bonaccorso, E.; Kappl, M.; Butt, H. J. Hydrodynamic force measurements: boundary slip of water on hydrophilic surfaces and electrokinetic effects. *Phys. Rev. Lett.* **2002**, *88*, 076103.

NL802931R